applied sciences

MDPI

Article

Prediction of Friction Coefficient for Ductile Cast Iron Using Artificial Neural Network Methodology Based on Experimental Investigation

Ahmad A. Khalaf and Muammel M. Hanon *

Middle Technical University (MTU), Baqubah Technical Institute, Baghdad 10074, Iraq
* Correspondence: muammel.m.hanon@mtu.edu.iq

Abstract: The key objective of the present study is to analyze the friction coefficient and wear rate for ductile cast iron. Three different microstructures were chosen upon which to perform the experimental tests under different sliding time, load, and sliding speed conditions. These specimens were perlite + ferrite, ferrite, and bainitic. Moreover, an artificial neural network (ANN) model was developed in order to predict the friction coefficient using a set of data collected during the experiments. The ANN model structure was made up of four input parameters (namely time, load, number, and nodule diameter) and one output parameter (friction coefficient). The Levenberg–Marquardt back-propagation algorithm was applied in the ANN model to train the data using feed-forward back propagation (FFBP). The results of the experiments revealed that the coefficient of friction reduced as the sliding speed increased under a constant load. Additionally, it exhibits the same pattern of action when the test is run with a heavy load and constant sliding speed. Additionally, when the sliding speed increased, the wear rate dropped. The results also show that the bainite structure is harder and wears less quickly than the ferrite structure. Additionally, the results pertaining to the ANN structure showed that a single hidden layer model is more accurate than a double hidden layer model. The highest performance in the validation stage, however, was observed at epochs 8 and 20, respectively, for a double hidden layer and at 0.012346 for a single layer at epoch 20.

Keywords: friction coefficient; wear rate; sliding speed; neural network

Citation: Khalaf, A.A.; Hanon, M.M. Prediction of Friction Coefficient for Ductile Cast Iron Using Artificial Neural Network Methodology Based on Experimental Investigation. *Appl. Sci.* **2022**, *12*, 11916. https://doi.org/10.3390/app122311916

Academic Editors: Rodolfo Haber, Krzysztof Ejsmont, Aamer Bilal Asghar and Yong Wang

Received: 20 October 2022
Accepted: 19 November 2022
Published: 22 November 2022

1. Introduction

The industrial problem of wear can significantly damage the overlapping components that move by each other [1]. There are a number of different factors that can impact the wear rate, including the metal hardness, sliding time and applied load [2]. Moreover, a number of methods can be used to reduce wear, such as applying lubricants to surfaces or using cast iron metal as it contains graphite pellets that can lubricate the surfaces of moving components [3]. Many academics have carried out experimental studies to investigate wear whilst also considering a variety of factors that have been identified in earlier studies [4,5]. Artificial intelligence (AI) technology has been developed over the last thirty years and has become one of the most popular ways to predict and overcome various engineering issues in different fields, particularly in industrial applications [6], as it can resolve and predict nonlinear relationships between the input and output parameters. Meanwhile, of all the AI machine learning approaches available, the artificial neural network (ANN) is considered to be one of the most important and popular [7].

ANNs were used to model and optimize various systems in the field of material science and this is primarily due to their flexibility and ability to understand problems without needing to know the exact details of the mathematical model. In fact, it does not even need to have information about the physical conditions. For instance, Radosaw et al. estimated the tensile strength of ductile iron friction welded joints using hybrid intelligence

methods [8]. The primary goal of their work was to use support vector regression (SVR), genetic algorithms (GA) and an imperialist competitive approach to maximize the welding parameters (ICA). The findings demonstrated that the TS of 256.93 MPa was achieved using SVR plus GA algorithms with heating force welding parameters of 40 kN, a heating time of 300 s, and an upsetting force of 10.12 kN. In addition, the use of hybrid intelligent approaches enhanced the TS joints from 211 to 258mpa for the ZT-14 type friction welder. Similarly, Vaira et al. used an ANN approach incorporating the Levenberg–Marquardt algorithm to predict the tensile strength of friction stir welded (FSW) for the AA1100 aluminum alloy [9]. Rotation speed, welding speed, shoulder diameter, and pin diameter were all applied as the ANN model's input parameters. The findings for the projected TS show that the ANN model is effective in predicting the tensile stress when these input parameters are present.

The mechanical characteristics of ductile cast iron were identified by Zmak et al., utilizing ANN based on the error back-propagation training technique [10]. The multilayer hidden layers of the ANN model had sigmoid activation functions. The 13 weights of chemical elements in melt were the input parameters used in the ANN model. Subsequently, the output included tensile and yield strength, hardness, and elongation. Additionally, Perzyk et al. built and trained a variety of ANN models to predict the quality of ductile cast iron and the findings indicated that ANN models are effective for use in melt shop on-line production control [11]. Furthermore, Anand et al. estimated the friction welding process parameters of Incoloy 800H joints and correlated the input and output responses of the friction welding using a hybrid ANN method incorporating the optimization algorithm [12]. It also explored how the best strength and hardness of joints can be achieved with the shortest burn-off length. The findings indicated that the friction welding process parameters may be accurately predicted using an ANN model combined with a genetic algorithm. Meanwhile, the friction coefficient and wear rate were examined in Kumar et al.'s study using an ANN model under the influence of various loads, pin heating temperature, and speed. The findings highlighted a significant relationship between the anticipated and measured values, with a correlation factor of 0.99447 [13]. However, a number of friction systems have employed ANN to design, forecast, and optimize friction parameters. By combining Elman's recurrent configuration with the ANN approach, Xiao and Zhu established several friction characteristics. The outcomes led to an improvement in material formulation, which was supported by evidence from research trials and experiments [14].

Additionally, ANN was employed by Aleksendric to predict the wear rate for friction materials. In his study, a number of different factors were considered, including (i) the formulation of the friction material (18 ingredients), (ii) the most critical manufacturing conditions for the friction material (5 parameters), (iii) the applied load and sliding velocity of the friction material (with both factors being represented by the work carried out through brake application) and (iv) the temperature of the brake interface [15]. In order to predict the corrosion potential and corrosion rate for the samples using the friction stir processing process parameters, Sai et al. proposed an ANN model containing a feed-forward backpropagation network and the Levenberg–Marquardt training algorithm [16]. With a coefficient of determination of unity, the ANN model was found to be in line with the experimental results. Moreover, Soni et al. investigated the prediction ability of tribological properties of nuclear grade graphite using the ANN model [17]. Meanwhile, Alyuda Neuro's intelligence software was employed to test the ANN model under different measured parameters, including time, temperature, sliding distance, and friction force. The findings revealed that the proposed ANN model and back-propagation Alyuda Neuro intelligence was able to effectively predict the frictional features of nuclear grade graphite with a correlation coefficient of 0.9995 and a mean absolute error of 0.0030%. Erosion wear was also predicted using various computational methods [18]. Although many studies in the literature, as presented above, have been accomplished for predicting the tribological behavior of different materials using the ANN approach. However, to our knowledge, no

one has investigated the forecasting of the tribological characteristics for ductile cast iron under dry conditions.

The key objective of this research is to examine the wear rate and friction coefficient for ductile cast iron. In order to carry out the experiments under the influence of sliding duration, load, and speed, three different microstructures were selected. These samples consisted of bainitic, ferrite, and perlite plus ferrite. Additionally, the ANN model based on the obtained data for the experimental testing was constructed to estimate the coefficient of friction using two structures.

2. Materials and Methods

2.1. Materials

Nine specimens of ductile cast iron measuring 20 mm in length and 10 mm in diameter were selected for use in this experiment. The chemical composition of the samples was determined using an optical emission spectrometer (branded SPECTROMAXx) for the chemical analysis to find the element percentages included in the composition of ductile cast iron, as listed in Table 1. The nine specimens exhibit a (perlite + ferrite) microstructure and a hardness of 180 HV. Figure 1 displays the ductile cast iron microstructure prior to etching (a). It is evident from Figure 1 that the microstructure of the specimens was created using the Nital solution, the latter of which contained both nitric acid and alcohol (2% HNO3 + 98% ALCOHOL) (b).

Table 1. The chemical composition of ductile cast iron.

Carbon	Silicon	Manganese	Magnesium	Phosphorus	Sulfur	Copper	Iron
3.25%	2.25%	0.14%	0.030%	0.005%	0.005%	0.32%	94%

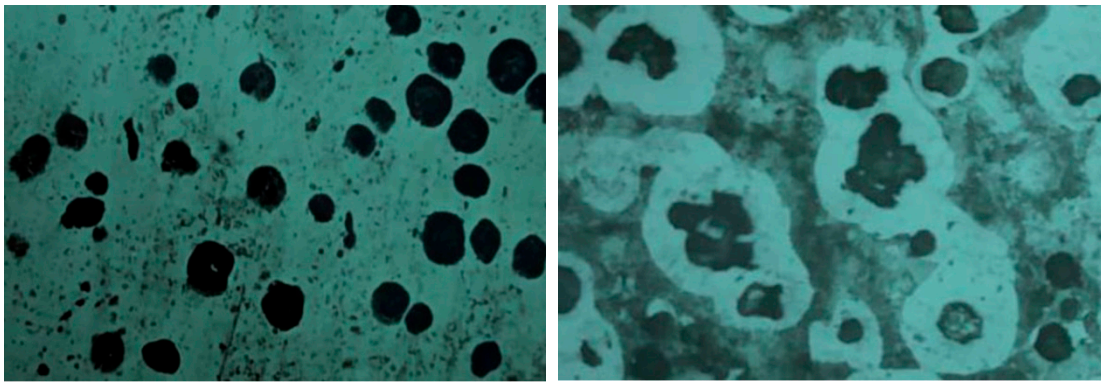

(**a**) (**b**)

Figure 1. Microstructure of ductile cast iron (**a**) before etching (**b**) after etching (Magnification: 136×).

2.2. Methods

2.2.1. Annealing

The three samples were heated to 900 °C for 60 min in order to obtain the ferrite microstructure, and they were subsequently cooled to room temperature after switching off the furnace. After annealing, the hardness test was conducted on the samples, and an average value of roughly 145 HV was obtained. Figure 2 presents the microstructural appearance of one ferrite specimen after annealing.

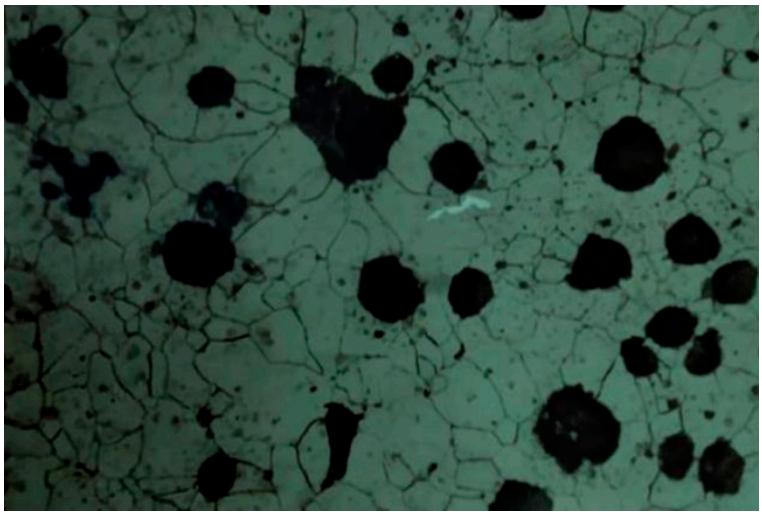

Figure 2. Ferrite microstructure (Magnification: 136×).

2.2.2. Austenitic (Isothermal) Process

The three specimens were heated to 950 °C for 60 min to perform an isothermal procedure the purpose of which was to produce the bainitic microstructure. The samples were then cooled again until they reached room temperature after being cooled in molten lead at 330 °C for 1 h. This was necessary to ensure that they initially reached the necessary melting temperature. After annealing, the hardness test was conducted on these specimens, and an average value of roughly 320 HV was obtained. Figure 3 depicts the microstructure of bainitic.

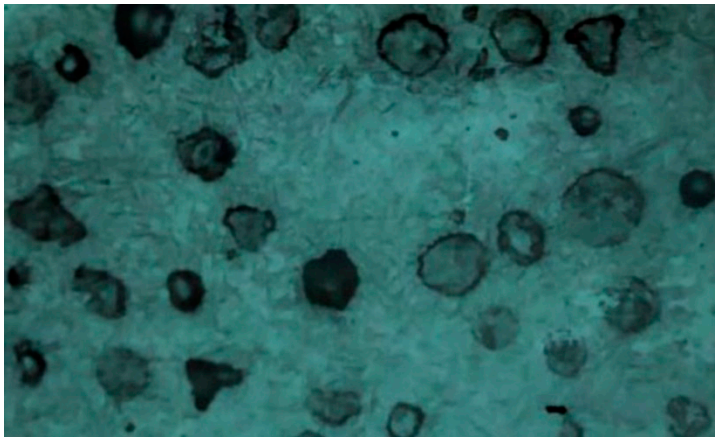

Figure 3. Bainitic microstructure (Magnification: 136×).

2.2.3. Sliding Wear Test

As illustrated in Figure 4, sliding wear was tested using a pin-on-disk device under dry sliding conditions to measure the coefficient of friction and wear rate. Three identical specimens were tested on each examined condition. It is noteworthy that friction and wear are properties of the whole system, not just the materials. In particular, the surface roughness greatly influences the results. However, in this work, the roughness for all sliding surfaces of testing specimens, as well as the sliding disk, was the same to allow the influence of other parameters to be investigated. Therefore, the specimens had been polished and smoothed to obtain a surface free of scratches. The surface roughness of the testing samples after polishing was 0.15 μm, while the surface roughness of the sliding disk after fine grinding was 0.35 μm. The roughness was determined using the Taly surf Talyor Hobson device for surface roughness measurement. Different loads with varying

devices, times, and microstructure parameters were applied to the specimens, after which the friction coefficients were calculated.

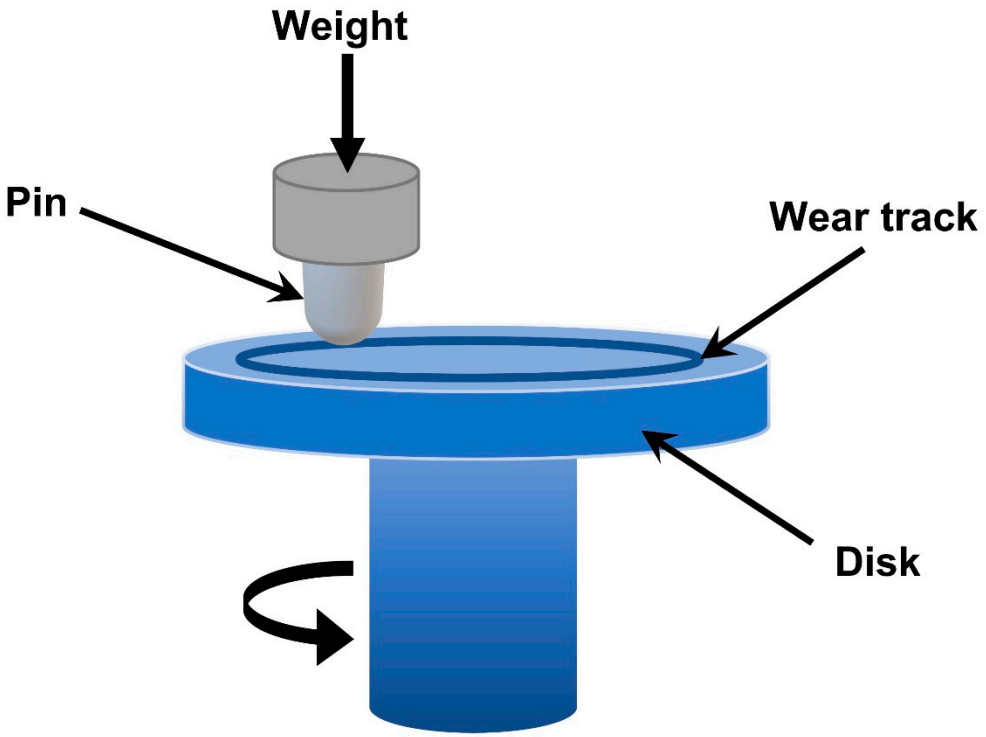

Figure 4. Schematic diagram of the pin-on-disk device.

To calculate the friction coefficient, Equation (1) was used [19]

$$\mu = \frac{F}{L} \tag{1}$$

In this equation, F represents the friction force (N), whilst L denotes the applied normal load (N)

The wear rate was determined using the weighing method by calculating the lost weight of the samples according to the following steps:

- Weighing the sample before each test using a sensitive balance with a sensitivity of 0.0001 g, where the weight of the specimen before the test was (3.0195 g);
- Determining the parameter whose effect is to be studied on the wear rate (e.g., sliding time) and fixing all other parameters (normal load and sliding speed);
- Installing the sample to be tested with the wear device, placing it perpendicular to the sliding disk, and then operating the device for specified periods. The piece is weighed after the test and to calculate the wear rate; Equation (2) was used [20]

$$WR = \frac{\Delta W}{ds} \tag{2}$$

In this equation, ΔW denotes the losses weight ($\Delta W = W_1 - W_2$), W_1 represents the specimen weight before the test, W_2 represents its weight after the test (g), and ds denotes the sliding distance (cm). Table 2 demonstrates the weight loss for one of the samples tested under specific operating conditions.

Table 2. Weight loss throughout testing one of the specimens.

Sliding Time (min)	Weight before Testing (g)	Weight after Testing (g)	Weight Loss (g)
5	3.0195	3.0192	0.0003
10	3.0192	3.0185	0.0007
15	3.0185	3.0176	0.0009
20	3.0176	3.0162	0.0014
25	3.0162	3.0146	0.0016
30	3.0146	3.0135	0.0011

3. Methodology of Artificial Neural Network

In linear and nonlinear systems, the relationship between input and output parameters can be predicted using the flexible and simple application known as the artificial neural network (ANN) [21,22]. Generally, it consists of three main layers: the first layer is the input layer where the input parameters are defined and connected between them by neurons, as shown in Figure 5 [23]. The weights and biases that make up the neurons were used to link the neurons, while the biases were used to determine the system's level of freedom. The second layer is a hidden layer (output layer) and the third layer contains the output parameters. The formula below (Equation (3)) can be used to work out the relationship between the input, weight, and output parameters [21].

$$net_j = \sum_{i=0}^{n} W_{ij} x_i + x_0 \tag{3}$$

$$Y_j = f_{act}(net_j) \tag{4}$$

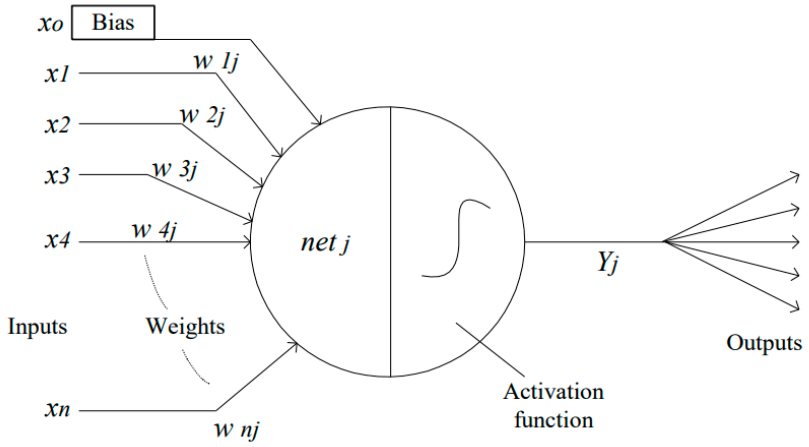

Figure 5. Individual neuron structure of the ANN [21].

In this equation, net_j represents the summation of multiplying each input x_i by weight W_{ij}, whilst x_0 denotes the bias, and n and j denote the number of inputs and neurons, respectively. The key purpose of the transfer function is to translate the signal from the hidden to the output layer and then to the final output. In ANN models, activation functions of the mathematical types linear, sigmoid, and hyperbolic tangent are used. The most popular of these activation functions is the sigmoid function (Equation (5)), which is discussed in [24]

$$f(S) = \frac{1}{1 + e^{-S}} \tag{5}$$

4. Results and Discussion

4.1. Experimental Results

An experiment was carried out to investigate how different loads, sliding times and sliding speeds impacted the friction coefficient and wear rate of ductile cast iron in a ferrite microstructure. Table 3 shows the exact specifications for these microstructures.

Table 3. Microstructure test characteristics.

Type	No. of Nodules (mm^2)	Diameter (μm)	Load (N)	Sliding Speed (cm/s)
Spec.1	355	20.9	17.338	70
Spec. 2	335	20.9	52.015	70
Spec. 3	335	20.9	52.015	114

In Figure 6, the extent to which the friction coefficients (COF) of the three specimens change as the sliding duration increases can be seen. Comparisons were made between specimens 2 and 3 to identify differences in how the COF behaves when the sliding speed changes (from 70 to 114 cm/s) and the load is kept constant (52.015 N). The findings show that there was a reduction in the COF when the sliding speed increased and the load remained constant. This can be summarized by saying that increased sliding speed causes the temperature between the two sliding surfaces to rise. Thus, at high sliding speeds, friction has less of an impact on the specimen's surface than it does at low sliding speeds.

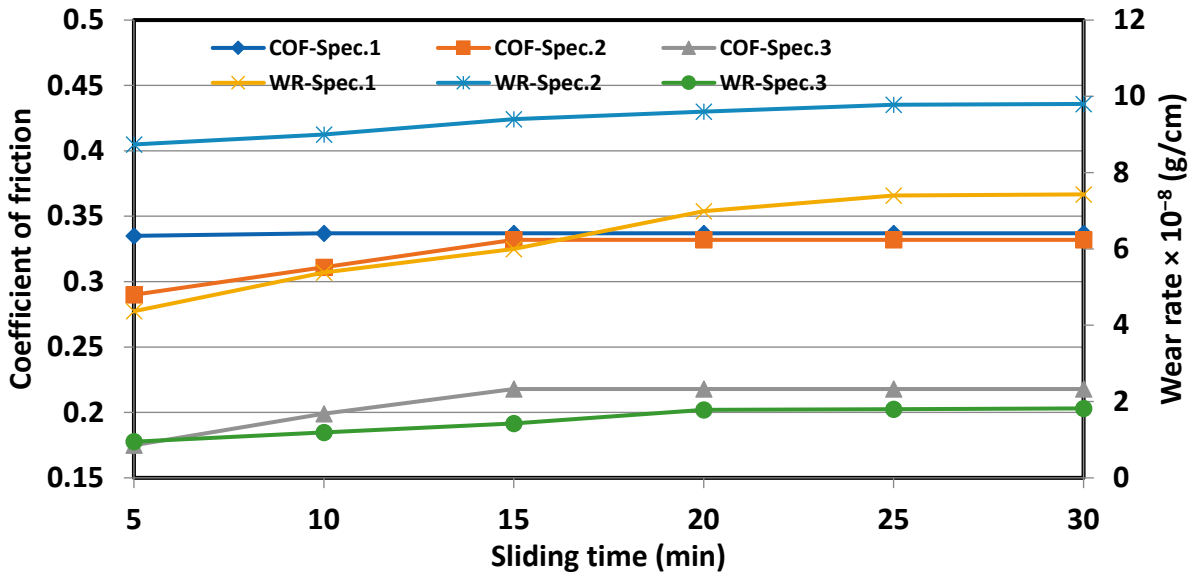

Figure 6. Differences in the friction coefficients and wear rates based on sliding time.

Additionally, Figure 6 compares specimen 2 and specimen 3 at sliding speed (70 to 114) cm/s and under constant load (52.015 N) in order to illustrate the behavior of wear rate (WR). It is evident that the wear rate dropped as the sliding speed increased. This can be explained by stating that friction caused the temperature between the two sliding surfaces to rise as the sliding speed increased. When sliding at a high speed, less heat is lost through the metal than when moving slowly, which promotes the development of an oxide layer that slows the rate of wear.

The effect of the applied load on the wear rate can be determined by fixing other parameters and varying the load. This is clearly demonstrated when comparing the behavior of specimen 1 and specimen 2 in Figure 6, which shows that the wear rate increases with the increase in the applied load. The reason for this is due to the increase in the plastic deformation that occurs between the two surfaces, thus increasing the real

area of contact. Furthermore, the high load leads to a strong metal contact that makes the force required to cut the connected protrusions higher than the strength of connecting metal atoms.

Figure 7 shows the impact of the microstructure produced by heat treatments (annealing and isothermal processes) on the wear rate. The sliding time was the variable parameter, while the other parameters (applied load and sliding speed) were kept constant. It is clearly shown in the figure that the bainite structure produced a lower wear rate than the ferrite structure. This is due to the fact that the resistance of the bainite structure's surface layers to plastic deformation is higher than the ferrite structure because of the bainite structure's higher hardness (320 HV). On the other hand, the ferrite structure's lower hardness (145 HV) generates a plastic flow and increases the size of the contact area. It also causes weak resistance due to its softness and readily adheres to the opposing surface [25].

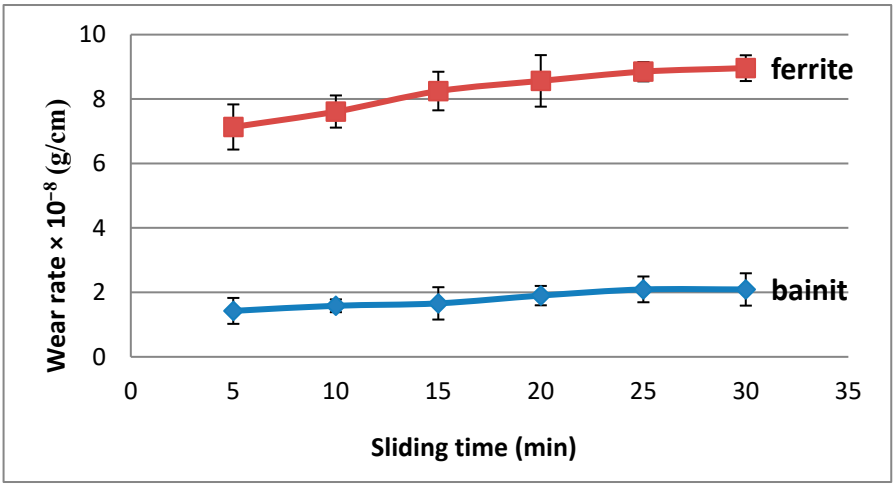

Figure 7. Effect of microstructure on the wear rate at a load of 52.015 N and sliding speed of 70 cm/s.

4.2. Data Collection and ANN Results

AAN was utilized to predict the coefficient of friction using MATLAB code that was executed on 81 measured data in the experiments. Table 4 displays samples of these data in tabulated form. The table displays both the input parameters (slide time, load, number of nodules, and nodule diameter) and the output parameter (coefficient of friction). Altogether, 30% of these datasets were applied to test and verify the model, whilst the remaining 70% were used to train the ANN model. Thus, 12 datasets were utilized for each testing and validation stage, while approximately 57 datasets were used for the training stage. The ANN model's specifications are summarized below:

- The use of the Levenberg–Marquardt back-propagation algorithm enabled the training stage to be reached;
- Two ANN structures were employed, one of which had a single hidden layer and the second of which contained a double hidden layer;
- To assess the ANN model, the mean squared error (MSE) and coefficient of determination (R^2) must be calculated;
- A trial-and-error technique was used to control the number of neurons in the hidden layer;
- The sigmoid function enabled the hidden layer to be activated, whilst the purline activation function was used to activate the output signal.

Table 4. Friction coefficients for different ductile cast-iron microstructures.

No.	Load (N)	Time (min)	Number of Grains/mm^2	Diameter of Grain (μm)	Friction Coefficient
1	17.33	5	256	30.6	0.293
2	17.33	10	256	30.6	0.356
3	17.33	15	256	30.6	0.356
4	17.33	20	256	30.6	0.356
5	17.33	25	256	30.6	0.356
6	17.33	30	256	30.6	0.356
7	34.67	5	256	30.6	0.325
8	34.67	10	256	30.6	0.346
9	34.67	15	256	30.6	0.393
10	34.67	20	256	30.6	0.393
11	34.67	25	256	30.6	0.393
12	34.67	30	256	30.6	0.393
13	52.01	5	256	30.6	0.314
14	52.01	10	256	30.6	0.321
15	52.01	15	256	30.6	0.335
16	34.67	5	429	20.5	0.168
17	34.67	10	429	20.5	0.189
18	34.67	15	429	20.5	0.211
19	34.67	20	429	20.5	0.211
20	34.67	25	429	20.5	0.211

4.2.1. Best Validation

The structures of the single and double hidden layers in the ANN model are presented as (4-10-1) and (4-10-10-1), respectively. The components of the structure indicate the number of input parameters (4), hidden layers (1 or 2), and output parameter (1). It can be seen that 10 neurons were recorded for the single and double hidden layers in the two architectures. Thus, final ANN structures can be expressed as (4-10-1) and (4-10-10-1) for single and double hidden layers, respectively (this is based on the number of input parameters, hidden layers, and output parameters). Meanwhile, as can be seen in Figure 8, the best validation was achieved at MSE values of 0.038333 at epoch 8 in the double hidden layer and 0.012346 at epoch 20 in the single layer. This suggests that the data were properly trained.

4.2.2. ANN Model Performance

Figure 9 depicted the ANN model's performance. The performance of single and double hidden layers is depicted in the image. It was evident that the coefficient of determination (R^2) for the training stage, testing stage, validation stage, and overall process was recorded as (0.99947, 0.999907, 0.99924, and 0.99936) accordingly. The R^2 value indicated that the database had been properly educated. Thus, the best performance for the validation stage was reported to be excellent at R^2 at 0.99924. This indicates that the ANN structure with a single hidden layer has a strong capacity to predict the friction coefficient under the aforementioned conditions, including the number of nodules, load, nodule diameter and sliding time. On the other hand, the determination coefficient for the ANN structure's double hidden layer was found to be 0.99841, 0.99878, 0.99902, and 0.99846 for the training, testing, and validation processes, respectively. When comparing the two structures' performances, it is obvious that the single layer structure performs better than the double hidden layer structure.

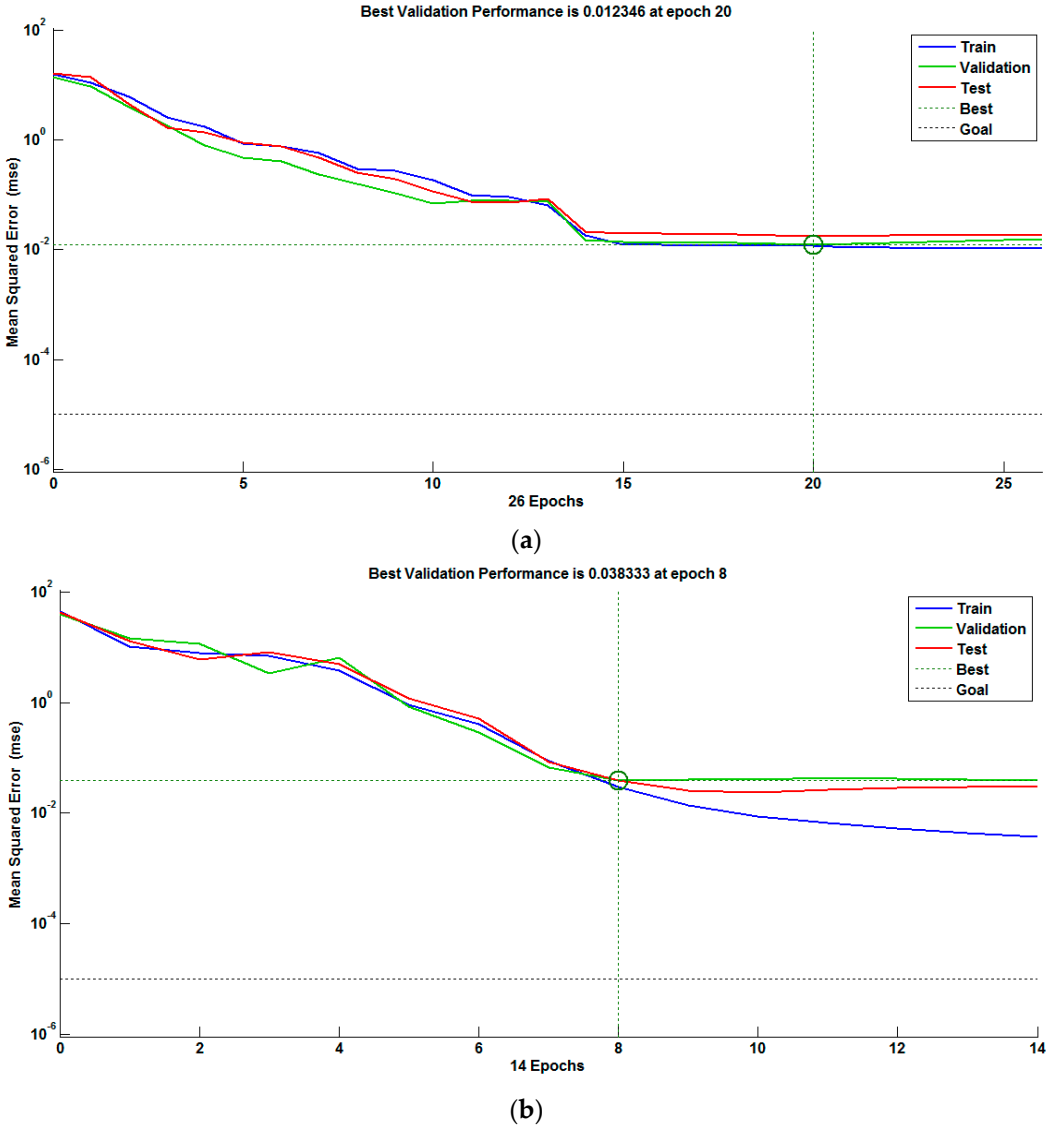

Figure 8. Best validation performance for the (**a**) single (**b**) double hidden layers.

4.3. Results Validation

The projected results for the two ANN structure models were confirmed through the measured outcomes from the training and validation phases. Altogether, 69 datasets were allocated over the two stages—57 for the training stage and 12 for the validation stage. As seen in Figure 10, in the case of an ANN with single and double hidden layers, the convergence between the predicted and observed coefficient of friction is precise. It is evident that the greatest values for the absolute error between the measured and predicted values in the single and double hidden layer architectures were 0.145 and 0.151, respectively. Thus, this strongly suggests that optimal accuracy has been achieved for the two ANN structures. Nonetheless, it is important to note that the single hidden layer has a more accurate structure.

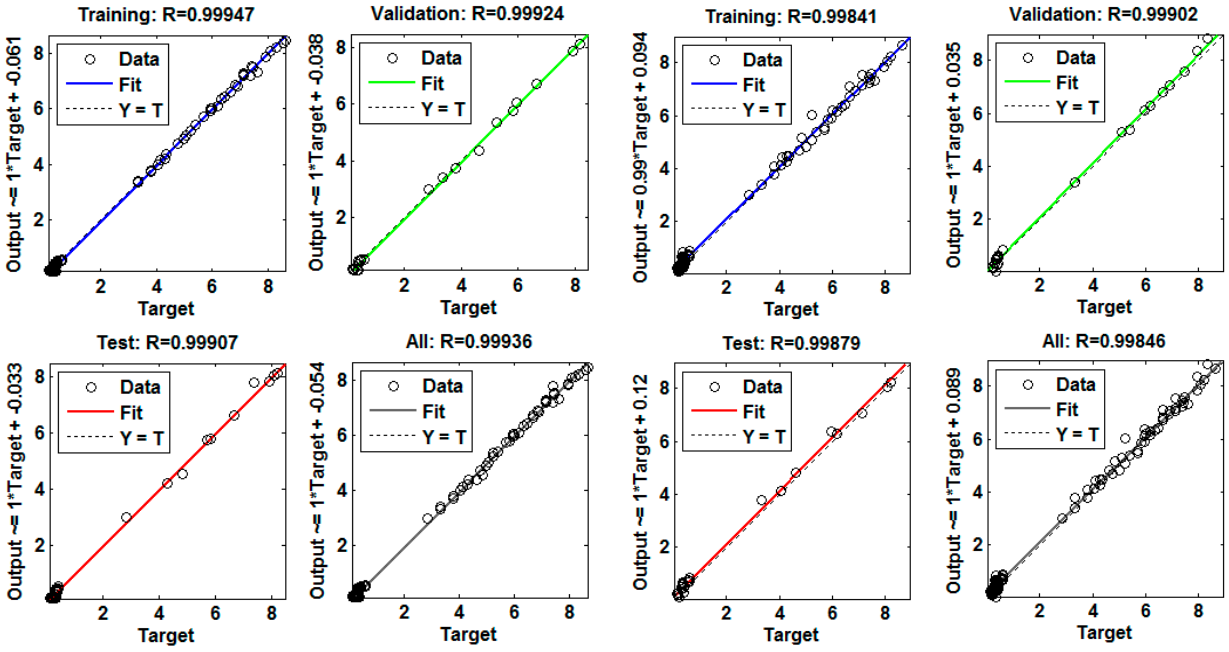

(**a**) (**b**)

Figure 9. ANN model performance at the four stages for (**a**) single (**b**) double hidden layer.

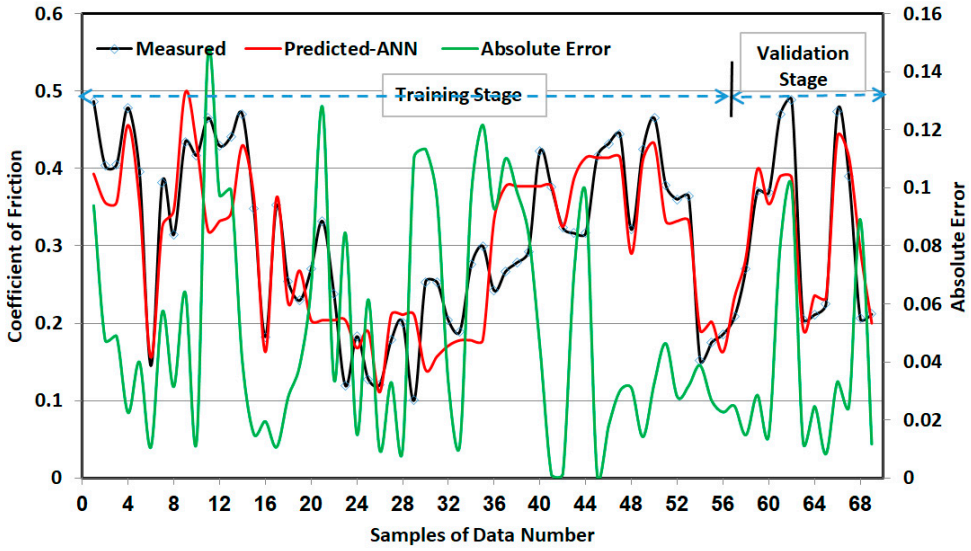

(**a**)

Figure 10. *Cont.*

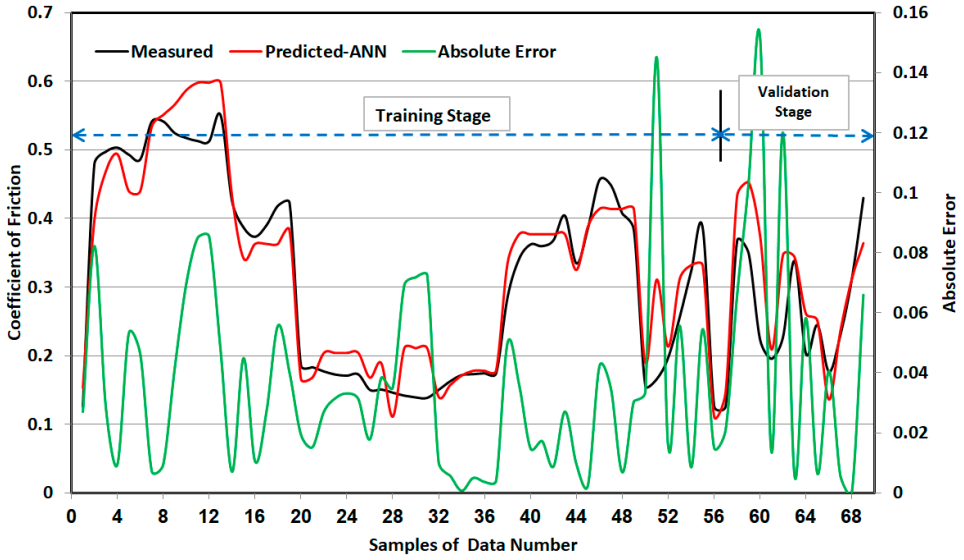

(**b**)

Figure 10. Comparisons between the predicted and actual friction coefficients for (**a**) single and (**b**) double hidden layers.

5. Conclusions

The key objective of this work was to evaluate the wear rate and friction coefficient for ductile cast iron. In order to perform the sliding duration, load, and speed conditions, three different microstructures were chosen. These samples were composed of bainitic, ferrite, and perlite plus ferrite. Additionally, the ANN model based on the obtained data for the experimental testing was constructed to estimate the coefficient of friction utilizing two structures. The research findings can be summarized in the following way:

- The COF decreased as the sliding speed increased under a constant load. Moreover, the COF displayed a similar pattern at a constant sliding speed under a high load;
- There was a reduction in the wear rate as the sliding speed increased. To be more precise, an increase in sliding speed from 70 cm/s to 114 cm/s caused a decline in the wear rate from (8.74 to 0.95) $\times$ 10^{-8} (g/cm) at the start of the experiment and from (9.8 to 1.82) $\times$ 10^{-8} (g/cm) at the end of the experiment;
- The wear rate increases with the increase in the applied load at constant sliding speed conditions due to the plastic deformation between the two surfaces, thus increasing the real contact area;
- The wear rate value was found to be lower for the bainite structure than the ferrite structure due to the higher hardness of the bainite structure;
- The ANN models with single and double hidden layers are able to accurately predict the friction coefficients;
- The ANN containing a single hidden layer was found to be more accurate than the that containing a double hidden layer. On the other hand, the best performance during the validation stage was recorded at an MSE of 0.012346 at epoch 20 in the single layer and 0.038333 at epoch 8 in the double hidden layer.

Since ductile cast iron is involved in a vast range of tribological applications in the industry, the findings of this research can be used by other investigators to forecast the wear rate and coefficient of friction for potential usages. In addition, the proposed model (ANN) is a simple architecture that researchers can develop as future work to predict the roughness of the sliding surfaces or the number of nodules for ductile cast iron.

Author Contributions: Conceptualization, A.A.K. and M.M.H.; methodology, A.A.K.; software, M.M.H.; validation, A.A.K. and M.M.H.; formal analysis, A.A.K.; investigation, A.A.K. and M.M.H.; resources, A.A.K.; data curation, A.A.K.; writing—original draft preparation, A.A.K.; writing—review and editing, A.A.K. and M.M.H.; visualization, A.A.K.; supervision, M.M.H.; project administration, A.A.K.; funding acquisition, A.A.K. All authors have read and agreed to the published version of the manuscript.

Funding: This research received no external funding.

Conflicts of Interest: The authors declare no conflict of interest.

References

1. Fan, Y.; Gui, X.; Liu, M.; Wang, X.; Bai, B.; Gao, G. Effect of Microstructure on Wear and Rolling Contact Fatigue Behaviors of Bainitic/Martensitic Rail Steels. *Wear* **2022**, *508–509*, 204474. [CrossRef]
2. Palavar, O.; Özyürek, D.; Kalyon, A. Artificial Neural Network Prediction of Aging Effects on the Wear Behavior of IN706 Superalloy. *Mater. Des.* **2015**, *82*, 164–172. [CrossRef]
3. Nayak, D.; Ray, N.; Sahoo, R.; Debata, M. Analysis of Tribological Performance of Cu Hybrid Composites Reinforced with Graphite and TiC Using Factorial Techniques. *Tribol. Trans.* **2014**, *57*, 908–918. [CrossRef]
4. Hanon, M.M.; Ghaly, A.; Zsidai, L.; Klébert, S. Tribological Characteristics of Digital Light Processing (DLP) 3D Printed Graphene/Resin Composite: Influence of Graphene Presence and Process Settings. *Mater. Des.* **2022**, *218*, 110718. [CrossRef]
5. Hanon, M.M.; Zsidai, L. Comprehending the Role of Process Parameters and Filament Color on the Structure and Tribological Performance of 3D Printed PLA. *J. Mater. Res. Technol.* **2021**, *15*, 647–660. [CrossRef]
6. Kazi, M.-K.; Eljack, F.; Mahdi, E. Predictive ANN Models for Varying Filler Content for Cotton Fiber/PVC Composites Based on Experimental Load Displacement Curves. *Compos. Struct.* **2020**, *254*, 112885. [CrossRef]
7. Arabi Bulaghi, Z.; Habibizad Navin, A.; Hosseinzadeh, M.; Rezaee, A. World Competitive Contest-Based Artificial Neural Network: A New Class-Specific Method for Classification of Clinical and Biological Datasets. *Genomics* **2021**, *113*, 541–552. [CrossRef]
8. Winiczenko, R.; Salat, R.; Awtoniuk, M. Estimation of Tensile Strength of Ductile Iron Friction Welded Joints Using Hybrid Intelligent Methods. *Trans. Nonferrous Met. Soc. China* **2013**, *23*, 385–391. [CrossRef]
9. Vaira Vignesh, R.; Padmanaban, R. Artificial Neural Network Model for Predicting the Tensile Strength of Friction Stir Welded Aluminium Alloy AA1100. *Mater. Today Proc.* **2018**, *5*, 16716–16723. [CrossRef]
10. Zmak, I.; Filetin, T. Mechanical Properties of Ductile Cast Iron Determined by Neural Networks. In Proceedings of the Third International Conference on Modeling, Simulation and Applied Optimization, Sharjah, United Arab Emirates, 20–22 January 2009; pp. 20–22.
11. Perzyk, M.; Kochański, A.W. Prediction of Ductile Cast Iron Quality by Artificial Neural Networks. *J. Mater. Process. Technol.* **2001**, *109*, 305–307. [CrossRef]
12. Anand, K.; Barik, B.K.; Tamilmannan, K.; Sathiya, P. Artificial Neural Network Modeling Studies to Predict the Friction Welding Process Parameters of Incoloy 800H Joints. *Eng. Sci. Technol.* **2015**, *18*, 394–407. [CrossRef]
13. Kumar, S.; Priyadarshan; Ghosh, S.K. Statistical and Artificial Neural Network Technique for Prediction of Performance in AlSi10Mg-MWCNT Based Composite Materials. *Mater. Chem. Phys.* **2021**, *273*, 125136. [CrossRef]
14. Xiao, G.; Zhu, Z. Friction Materials Development by Using DOE/RSM and Artificial Neural Network. *Tribol. Int.* **2010**, *43*, 218–227. [CrossRef]
15. Aleksendrić, D. Neural Network Prediction of Brake Friction Materials Wear. *Wear* **2010**, *268*, 117–125. [CrossRef]
16. Prudhvi Sai, P.; Roshan Balu, T.M.B.; Vaira Vignesh, R.; Bhaskara Sastry, C.V.; Padmanaban, R. Artificial Neural Network Models for Predicting the Corrosion Behavior of Friction Stir Processed AA5083. *Mater. Today Proc.* **2021**, *46*, 7215–7219. [CrossRef]
17. Soni, A.; Yusuf, M.; Beg, M.; Hashmi, A.W. An Application of Artificial Neural Network (ANN) to Predict the Friction Coefficient of Nuclear Grade Graphite. *Mater. Today Proc.* **2022**, *68*, 701–709. [CrossRef]
18. El-Emam, M.A.; Zhou, L.; Yasser, E.; Bai, L.; Shi, W. Computational Methods of Erosion Wear in Centrifugal Pump: A State-of-the-Art Review. *Arch. Comput. Methods Eng.* **2022**, *29*, 3789–3814. [CrossRef]
19. Tsukizoe, T.; Ohmae, N. Friction and Wear of Advanced Composite Materials. *Fibre Sci. Technol.* **1983**, *18*, 265–286. [CrossRef]
20. Nordin, N.A.; Yussof, F.M.; Kasolang, S.; Salleh, Z.; Ahmad, M.A. Wear Rate of Natural Fibre: Long Kenaf Composite. *Procedia Eng.* **2013**, *68*, 145–151. [CrossRef]
21. Mohd Noor, C.W.; Mamat, R.; Najafi, G.; Mat Yasin, M.H.; Ihsan, C.K.; Noor, M.M. Prediction of Marine Diesel Engine Performance by Using Artificial Neural Network Model. *J. Mech. Eng. Sci.* **2016**, *10*, 1917–1930. [CrossRef]
22. Pontes, F.J.; de Paiva, A.P.; Balestrassi, P.P.; Ferreira, J.R.; Silva, M.B. da Optimization of Radial Basis Function Neural Network Employed for Prediction of Surface Roughness in Hard Turning Process Using Taguchi's Orthogonal Arrays. *Expert. Syst. Appl.* **2012**, *39*, 7776–7787. [CrossRef]
23. Vastrad, C. Performance Analysis of Neural Network Models for Oxazolines and Oxazoles Derivatives Descriptor Dataset. *arXiv* **2013**, arXiv:1312.2853.

24. Ahmadi, M.H.; Baghban, A.; Sadeghzadeh, M.; Zamen, M.; Mosavi, A.; Shamshirband, S.; Kumar, R.; Mohammadi-Khanaposhtani, M. Evaluation of Electrical Efficiency of Photovoltaic Thermal Solar Collector. *Eng. Appl. Comput. Fluid Mech.* **2020**, *14*, 545–565. [CrossRef]
25. Ameen, H.A.; Hassan, K.S.; Mubarak, E.M.M.; Ameen, H.A.; Hassan, K.S.; Mubarak, E.M.M. Effect of Loads, Sliding Speeds and Times on the Wear Rate for Different Materials. *Am. J. Sci. Ind. Res.* **2011**, *2*, 99–106. [CrossRef]